Proceedings of 10th International Conference on Precision, Meso, Micro and Nano Engineering (COPEN 10)
December 07 – 09, 2017, Indian Institute of Technology Madras, Chennai – 600 036 INDIA

Numerical Simulation and Experimental Investigation of the Crater Surface Profiles Formed During Micro EDM on Inconel 718

Ananthan S P.[1], Deepak G Dilip*.[2], Satyananda Panda.[3], Jose Mathew.[4]
[1, 2, 4] Department of Mechanical Engineering, National Institute of Technology Calicut, 673601, India
[3] Department of Mathematics, National Institute of Technology Calicut, 673601, India

Abstract
Micro-EDM, owing to its ability to machine any electrically conductive material irrespective of their mechanical properties has great significance in the present manufacturing scenario. Before improving the existing process, a thorough understanding of the process physics is important. The aim of the present work is to compare the surface profile of the crater formed during single-spark micro electric discharge machining (µ-EDM) with the numerically simulated crater profiles. For this, numeric simulation of the crater geometry was done in ANSYS Fluent on the two-dimensional axi-symmetric model, for two distinct voltages and one value of capacitance. It utilises the Gaussian distribution of heat flux, fixed percentage of heat input to workpiece and fixed properties of the work material (Inconel 718 alloy). The effect of movement of the molten fluid layer in shaping the crater profile has been analysed by the simultaneous solution of heat, momentum and continuity equations following SIMPLE algorithm. Source terms were incorporated into the governing equations for the analysis of mushy zone. The experimental crater dimensions including the surface profiles were measured using 3D surface profiler. The surface profile of simulated craters has been plotted graphically and was compared with experimental profiles with an error less than 20%.

Keywords: Micromachining, µ-EDM, miniaturization, Inconel 718, mushy zone, ANSYS

1. INTRODUCTION

Electro Discharge Machining (EDM) is a thermal material removal process which removes material by melting and partly vaporizing by the action of sparking. The µ-EDM, a variant of EDM removes the material in the subgrain size range (0.1-10 µm). Most of the modeling work in µ-EDM evaluated the process of melting of workpiece material and compared the crater dimensions with the experimental results. But works related to the analysis of molten liquid motion in the melt pool and behaviour of material in the mushy zone was not considered enough. So the aim of this work is to develop a suitable model which can effectively predict the surface profile of the final crater formed in µ-EDM of Inconel 718.

Many research works have been carried out for modeling the mechanisms involved in the melting process of µ-EDM. Most of the works concentrated on the parameters of the crater formed as a result of melting. Joshi and Pande [1] developed a single spark thermo-physical model for die sinking electro discharge machining using 2D finite element method. It was based on more realistic assumptions such as the Gaussian distribution of heat flux, spark radius equation based on discharge current and discharge duration, latent heat of melting, etc. Effect of various operating conditions on crater parameters was also studied. Tao et al. [2] presented a model for material removal in EDM, by considering bubble collapsing phase. The analysis was done considering the mushy zone. The simulations were done using CFD package Fluent. The simulation and experiment results conditions showed good agreement for crater diameter. Somashekhar et al. [3] proposed an electro-thermal theory approach for numerical approximation of the micro-EDM process and reported the temperature distribution along the radius and depth of the stainless steel workpiece. Since µ-EDM is aimed at generating more precise products rather than increased MRR, the energy input per spark is reduced in µ-EDM [3] as compared with that of EDM [1]. The overall process physics and the methodology to calculate the crater dimension based on the temperature distribution remains more or less the same. Mujumdar et al. [4] developed a µ-EDM melt-pool model to predict workpiece (anode) material removal from a single discharge µ-EDM process. They took into account the process of melting and melt pool formation during the phase change from solid to liquid phase. It was observed that the diameters of the simulated craters agree reasonably well with the corresponding experimental measurements for almost all the discharge conditions. Voller et al. [5] developed an enthalpy formulation based fixed grid methodology for the numerical solution of convection-diffusion controlled mushy region phase-change problems. Versteeg and Malalasekera [6] mentioned about the usage of the staggered grid and the analysis of coupled equations using the SIMPLE algorithm. Patanakar [7] mentioned about the numerical analysis of coupled equations of heat and fluid flow. Yang et al. [8] modeled the melting process in laser processing using fixed meshes. The mixture of solid and liquid phases was analysed by modifying continuity, momentum and energy equations. The analysis was performed on AISI 304 stainless steel. The Marangoni effect was included into the velocity boundary conditions. Rahman et al. [9] mentioned about the physical properties of Inconel 718 and its difficulties in machining compared to conventional methods. Mills [10] provided detailed description about the thermophysical properties of Inconel 718. The relationship for obtaining the properties in the mushy zone in terms of temperature and solid fraction was presented. Romano et al. [11] presented a model for simulating fabrication of Inconel 718 using laser melting process. Detailed changes in properties with temperature were incorporated in the model. Saunders et al. [12] presented the properties and behaviour of Nickel alloys in the various range of temperature. The variation in the properties like density and dynamic viscosity over the mushy zone temperature is presented graphically for Inconel 718.

This paper presents a simulation of the melting of Inconel 718 during µ-EDM process. The model was solved using SIMPLE algorithm incorporating the effects of the mushy zone

*deepakgd1@yahoo.co.in

ISBN: 978-93-80689-28-9

in the melting of alloy using enthalpy porosity method. The model was formulated using the CFD package ANSYS Fluent. The surface profile of the crater formed by different conditions of voltage and capacitance are obtained from the simulation. An experimental validation is done for the same range of voltage and capacitance. The profiles of the crater formed are measured and have been compared with those obtained from the simulation.

2. INCONEL 718

Inconel 718 is a nickel-based superalloy. It finds its main application in the aerospace industry particularly in the hot sections of gas turbines of the jet engines. Inconel 718 has highly promising properties like very high strength, excellent corrosion and thermal resistance while its machinability is very poor. Instead of conventional machining, non-conventional processes are mostly preferred for its machining.

As Inconel 718 is an alloy, it does not have a single value of melting point. The solidus temperature of the alloy is 1523K and liquids temperature is 1619K. In between these two temperatures, the alloy shows a semisolid behaviour. This zone is called mushy zone. The properties of Inconel 718 in this zone are calculated separately based on the liquid fraction, solidus and liquidus temperature.

2.1 Thermophysical Property Calculations

The properties of Inconel 718 in the mushy zone (1523-1619K) are calculated based on the solid fraction which is calculated based on the temperature at that point. In order to calculate the solid fraction there are three temperature ranges.

Range 1: Below solidus temperature (1523K)

Solid Fraction, $F_s = 1$

Range 2: Mushy Zone(T = 1523K – 1619K)

$$\boldsymbol{F_s} = -248.472774614688 + (0.327443760997081)\,T - (0.000107451712369228)T^2 \quad (1)$$

$$\boldsymbol{C_p} = F_s(C_{p\,solidus}) + (1 - F_s)\,C_{p\,liquidus}$$

$$\boldsymbol{K} = F_s(K_{solidus}) + (1 - F_s)\,K_{liquidus}$$

$$\boldsymbol{\rho} = F_s(\rho_{solidus}) + (1 - F_s)\rho_{liquidus}$$

$$\boldsymbol{\mu} = (0.00000006)T^2 - (0.0002)T + 0.205$$

where $X_{solidus}$ and $X_{liquidus}$ represent the value of any property X at the solidus and liquidus temperature respectively. All the properties in the mushy zone except dynamic viscosity are calculated based on the value of the properties at solidus and liquidus temperature. These properties are shown in Table 1.

Range 3: Above liquidus temperature (1619K)

Solid Fraction, $F_s = 0$

Table 1
Properties at mushy zone boundaries

Properties	At solidus temperature	At liquidus temperature
Thermal conductivity (W/m-K)	30	444
Specific heat (J/Kg-k)	666	720
Density (kg/m^3)	7705	7400

2.2. Initialisation of Properties

Temperature = 293K, Pressure = 1atm, Thermal conductivity = 11.4W/m-K, Specific heat = 435J/kg-K, Density = 8190 kg/m^3. The property input for the analysis was given as user defined function in ANSYS Fluent.

3. SIMULATION APPROACH

3.1. Work Domain

The domain of work is a square region of size 100μm × 100μm. It is being discretized into a grid of size 0.5μm × 0.5μm in the fine mesh region as the heat flux is incident at this region and minute variation of temperature needs to be studied, and 1μm × 1μm in the coarse meshed region. The work domain is as shown in Fig. 1.

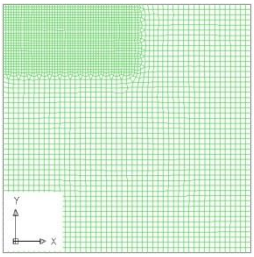

Fig.1. Work domain for ANSYS Fluent

3.2. Governing Equations

The governing equations used in this analysis are

3.2.1. Heat equation

$$\frac{\partial}{\partial t}(\rho h) + \nabla.(\rho \boldsymbol{V} h) = \nabla.(K \nabla h) + S_h \quad (2)$$

Here $h(t, x, y)$ represents the specific enthalpy variable defined at position (x, y) of the material and at time t. The symbols ρ and K represents the density and thermal conductivity of the material which are function of temperature T. The term $\frac{\partial}{\partial t}(\rho h)$ incorporates the transient effect of heat distribution into the analysis. Second term $\nabla.(\rho \mathbf{V} h)$ shows the advection effect. The effect of velocity maintains the heat flow due to convection. The conduction mode of heat transfer due to temperature gradient is represented by $\nabla.(K \nabla h)$. In the advection term $\boldsymbol{V} = (u, v)$ represents the total velocity of the flow. Finally, the source term is included to incorporate the effect of latent heat. The source term

$$S_h = \frac{\partial(\rho \lambda L)}{\partial t} + \nabla.(\rho \boldsymbol{V} \lambda L), \quad (3)$$

where, L represents the latent heat of the material which is 250000 J/kg and λ represents the liquid fraction of the cell given by $\lambda = (1 - F_s)$, where F_s is the solid fraction of the cell. While melting, when the material undergoes phase change, the temperature remains constant. So the source term act as a heat sink. It also incorporates the effect of fluid motion in the mushy zone with the velocity term.

3.2.2. Conservation of momentum

In x direction

$$\frac{\partial(\rho u)}{\partial t} + \nabla.(\rho \boldsymbol{V} u) = -\frac{\partial p}{\partial x} + \nabla.(\mu \nabla u) + S_x \quad (4)$$

In y direction

$$\frac{\partial(\rho v)}{\partial t} + \nabla.(\rho \mathbf{V} v) = -\frac{\partial p}{\partial y} + \nabla.(\mu \nabla v) + S_y \quad (5)$$

The terms involved are transient, convection, pressure gradient, diffusion and source.Here the source terms is given by
$S_x = -Au$, for x component of momentum
$S_y = -Av$, for y component of momentum

Here $A = C(1-\lambda)^2/(\lambda^3+q)$, where C is a constant that depends on the morphology of the porous medium. The value of C is set 1.6×10^3 and q is chosen a value 0.001 to avoid division by zero [4]. The source term is introduced to manipulate the use of momentum equation in the three phases of the melting process.

In the solid state $\lambda = 0$, the value of A will be sufficiently high. This will result in the generation of a very low velocity from the momentum equation solution. In the liquid phase, $\lambda = 1$, A will become zero, thus no modification for the momentum equation will happen. But in the mushy zone, $0 < \lambda < 1$, A will have a significant range of values which alters the momentum equation to make the analysis suitable in the mushy zone. The mushy zone is analysed as a porous medium with the porosity same as the liquid fraction of the cell.

3.*2.3. Continuity equation*

$$\frac{\partial \rho}{\partial t} + \frac{\partial \rho u}{\partial x} + \frac{\partial \rho v}{\partial y} = 0 \qquad (6)$$

This is used to ensure that the velocities calculated from the momentum equations are properly corrected. The correction pressure is obtained from modifying the continuity equation.

3.2. Solution Methodology

The scheme used for pressure-velocity coupling is SIMPLE algorithm. The pressure in the domain is discretized linearly; first order upwind scheme is followed for energy and momentum discretization. The under-relaxation factor for pressure calculation is taken as 0.3 and for velocity calculation, it is taken as 0.4.

3.3. Boundary Conditions

During the µ-EDM process, once the spark hits the anode, the surface gets heated up and results in the melting of surface and subsurface layers. The thermal and velocity boundary conditions for the problem are shown below.

3.4.1. Thermal boundary conditions.

The workpiece for analysis is assumed to be axisymmetric and only quarter of the workpiece is analysed. Fig. 2 shows the thermal boundary condition used.

At boundary 1 i.e. the top surface two conditions are applied. A Gaussian heat flux is applied up to the spark radius R and a convective heat flux is applied on the remaining region during the spark on time which is given by

$$K\frac{\partial T}{\partial y} = \begin{Bmatrix} q_r\,,\ x \le R \\ h_c(T-T_a), x > R \end{Bmatrix} \qquad (7)$$

where the variable r is the radius at any point on the surface of the workpiece, R is the spark radius, h_c is the heat transfer coefficient and q_r is the varying heat flux intensity defined as

$$q_r = 3.157 q_0 e^{-3\left(\frac{r}{R}\right)^2}, \qquad (8)$$

q_0 represents the amount of heat transferred to the workpiece given by the expression

$$q_0 = \frac{\eta E}{\pi R^2 t_{on}}, \qquad (9)$$

where η is the percentage of heat transferred to the workpiece, t_{on} is the pulse on time and E is the energy dissipated.

In the case of an RC circuit based µ-EDM, the energy produced per spark is given by

$$E = \frac{1}{2}CV^2, \qquad (10)$$

where C is the capacitance and V is the gap voltage.

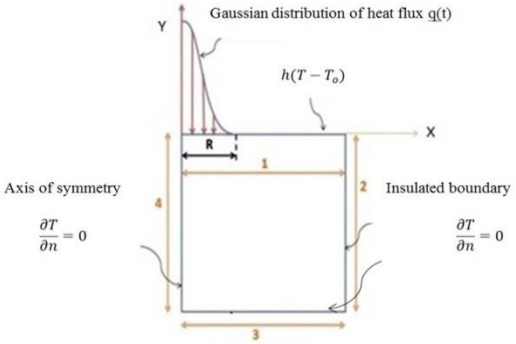

Fig.2. Thermal boundary conditions

All other edges are insulated given by

$$K\frac{\partial T}{\partial \boldsymbol{n}} = 0, \qquad (11)$$

where $\boldsymbol{n}$ represents the unit normal vector to the surface of the workpiece. During pulse off time, the entire condition of boundary 1 is

$$K\frac{\partial T}{\partial y} = h_c(T - T_a) \qquad (12)$$

The value of heat transfer coefficient is taken to be 1000W/m^2K during t_{on} and t_{off}.

3.4.2 Velocity boundary conditions.

Initially, as the material considered is in a solid state at room temperature, all the velocities within the grid are taken to be zero. Once the µ-EDM process starts, it results in the formation of liquid layer at the top due to melting and hence the boundary condition also changes. At the boundary 2, 3, 4 the velocity gradient in the normal direction to the surface is set to be zero. At the top surface i.e., boundary 1 once the liquid formation starts, the surface tension of the liquid-gas interface also comes into the picture. Due to the temperature difference existing at the surface, it creates a gradient of surface tension. This surface tension (σ) gradient generates a tangential force which will get balanced by the viscous force of the flow due to shear. This mode of stress is called Marangoni stress [7] and is given by

$$-\mu\frac{du}{dy} = \frac{d\sigma}{dT} \times \frac{dT}{dx} \qquad (13)$$

3.5. Assumptions involved

1. The material is homogeneous and isotropic
2. The model considered is axi-symmetric about y axis and single spark model considered
3. Heat transfer by conduction and convection only
4. Heat flux is Gaussian distributed
5. Flushing efficiency is 100 percentage
6. A fraction of total heat only reaches anode

3.6. Melting and Solidification

Melting and solidification module available in ANSYS Fluent is made used for simulating the rapid melting process during the discharge. This module supports the simulation of melting in alloys by using enthalpy porosity method.

4. RESULTS AND DISCUSSIONS

Table 3 shows the crater radius (R) and crater depth (D) for voltage of 100 V and 125 V and capacitance 0.4 µF.

Table 3
Simulation results

Set	Voltage (V)	Capacitance (µF)	R (µm)	D (µm)
I	100	0.4	27.37	11.68
II	125	0.4	31.62	14.52

Simulation of the process was done for two sets of voltage and one set of capacitance. Fig. 3 shows the Temperature contour in Kelvin for the condition V = 100V and C = 0.4µF. The crater geometry is plotted and we can see that a realistic irregular shape is obtained.

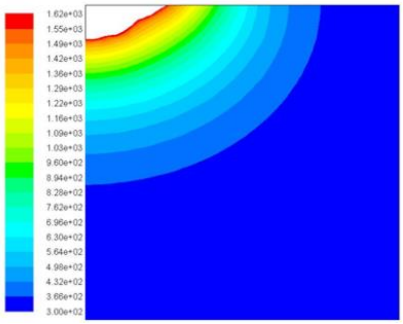

Fig. 3 Temperature contour at V= 100V and C = 0.4µF

The experiment was conducted for the same set of conditions mentioned in Table 3 using micromachining centre. The tool used is Tungsten Carbide of 400 µm diameter and work material is Inconel 718. The profile of the crater surface obtained from the simulation work had been compared with the profiles obtained from the experimental results. The comparison shows how well the model was able to predict the surface texture of the crater formed during µ-EDM of Inconel 718. The percentage deviation between the profiles are calculated and a mean value is estimated which quantifies the deviation. Fig. 4 shows the profile comparison for V = 100V and C=0.4µF. Similar comparison was done for two sets mentioned earlier. The mean deviations between profiles are shown in Table 4.

Table 4
Surface profile comparison data

Set	Mean deviation (%)
I	10.57
II	15.791

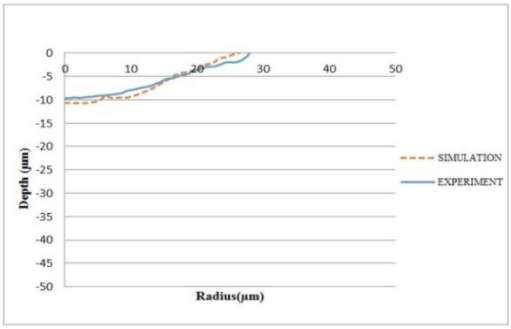

Fig. 4 Comparison profile for V =100V and C =0.4µF

5. CONCLUSIONS

The shape of the crater is in good agreement with the actual shape obtained from experimental results. The surface irregularities generated due to the inclusion of fluid motion in the simulation is well justified in this work.

The surface profile predicted by simulation is having a deviation of 10.57% and 15.79% in comparison with the experimental results.

Acknowledgment

Authors would like to sincerely thanks Department of Science & Technology(DST), Govt. of India & Centre for Precision Measurements & Nanomechanical Testing , Department of Mechanical Engineering , National Institute of Technology Calicut , for providing support to carry out this work under the scheme ‘Fund for improvement of Science & Technology’ (No. SR/FST/ETI-388/2015).

References

[1] Joshi. S. N., and Pande. S. S., “Thermo-physical Modeling of Die-sinking EDM Process,” *J. Manuf. Process*., **12** (1) (2010) 45-56.

[2] Tao. J., Ni. J., and Shih. J.A., “Modelling of the Anode Crater Formation in Electrical Discharge Machining,” *ASME. J. Manuf. Sci. Eng*., **134** (2012) 011002-1 - 011002-11.

[3] Somashekhar. K.P., Mathew. J., and Ramachandran. N., “Electrothermal Theory Approach for Numerical Approximation of the µ-EDM Process,” *Int. J. Adv. Manuf. Technol*., **61** (2012) 1241–1246

[4] Mujumdar. S. S., Curreli. D., Kapoor. S. G., and Ruzic. D., “Modeling of Melt-Pool Formation and Material Removal in Micro-Electrodischarge Machining*,” ASME. J. Manuf. Sci. Eng*., **137** (3) (2015) 031007-1 - 031007-9.

[5] Voller. R. V., and Prakash. C., “A Fixed grid numerical modeling methodology for convection-diffusion mushy region phase-change problems,” *Int. J. Heat Mass Transfer*., **30** (8) (1987) 1709-1719.

[6] Versteeg. H. K., and Malalasekera. W., “An Introduction to Computational Fluid Dynamics The Finite Volume Method,” *PEARSON Prentice Hall, Harlow,* (2007)

[7] Patanakar. V. S., “Numerical Heat Transfer and Fluid Flow,” *Taylor & Francis, USA*.(1980)

[8] Yang. L. X., Peng. X. F., and Wang. B. X., “Numerical modeling and experimental investigation on the characteristics of molten pool during laser processing,” *Int. J. Heat Mass Transfer*., **44** (2001) 4465-4473.

[9] Rahman. M., Seah. W. K. H., and Teo. T.T., “The Machinability of Incone1 718,” *J. Mater. Process Technol*., **63** (1997) 199-204.

[10] Mills. C. K., “Recommended values of thermophysical properties for selected commercial alloys,” *Woodhead Publishing Limited, Cambridge.*(2002)

[11] Romano. J., Ladani. L., and Sadowski. M., “Laser Additive Melting and Solidification of Inconel 718: Finite Element Simulation and Experiment,” *Min. Met. Mat. Soc.*, (2016) DOI:10.1007/s11837-015-1765-1.

[12] Saunders. N., Guo. Z., Li. X., Miodownik. A. P., and Schille. J. P., “Modelling the material properties and behaviour of Ni-based superalloys,” *Superalloys*, (2004) 849-858